

Effect of Iron Carbide on the Morphology and Protectiveness of Iron Sulfide Layer

Ezechukwu Anyanwu*, Bruce Brown, and Marc Singer
Institute for Corrosion and Multiphase Technology, Ohio University
342 West State Street
Athens, OH, 45701
USA

ABSTRACT

Carbon steel is mostly used as the material for oil and gas pipelines because of its economic advantage over other steel alloys. Due to the structural demands of oil and gas exploration on pipeline materials and oil country tubular goods (OCTG), the microstructure of carbon steel is often adjusted through carefully designed heat treatments to achieve more desirable mechanical properties. While it is important to optimize the structural properties of carbon steel, it is also necessary to understand how the resulting microstructure affects corrosion and formation of corrosion product layers. The effect of ferritic/pearlitic microstructure on formation of iron sulfide was investigated in this study. This microstructure was chosen based on the relatively wide use of UNS G10180 steel in different oil and gas production applications.

More specifically, the impact of cementite, present in the pearlite microconstituent of the ferritic/pearlitic microstructure, on the corrosion behavior in sour environment was investigated by using two substrates: UNS G10180 and 99.9% pure Fe. These substrates were exposed to brine solutions saturated with 10% by volume of H₂S in a mixture with nitrogen, at temperature of 30°C and pH of 5 and 6 for a period of 4 days. The morphologies of the FeS layers that developed after 1 day, 3 days and 4 days exposure were compared, and the changes in corrosion of each substrate were established from the monitored corrosion rates during these exposure periods. The corrosion product layers were analyzed using EDS and XRD in order to determine the composition of the corrosion product layers. Furthermore, the surface of the substrates was examined after removal of the corrosion product layers for possible localized attacks. SEM analysis of the corrosion product layers showed that the presence of cementite affected the morphology of the FeS layers formed on UNS G10180 with higher precipitation occurring in the pearlite region. The sharper decrease in the corrosion rates observed with UNS G10180 suggests that these layers became protective quicker than those that formed on the pure Fe substrate. The findings from this study were compared to the observation of other researchers when ferritic/pearlitic UNSG 10180 steel was exposed to CO₂ environment.

* Now at Exponent, Materials and Corrosion Engineering Practice, 149 Commonwealth Drive Menlo Park, CA, 94025

INTRODUCTION

The degradation of carbon steel materials used to construct oil and gas pipelines is of immense concern to both production and corrosion engineers, as well as metallurgists. For this reason, significant resources have been devoted to enhancing the corrosion resistance and mechanical strength of these steels. By modifying their microstructure, usually through careful heat treatments and alloying elements addition, carbon steels can be designed to better withstand the performance demands encountered in oil and gas applications.^{1,2} Furthermore, modification of steel microstructure may also impact the general corrosion behavior of such steels.³⁻⁵ For example, a heat treatment which results in the formation of distinct phases and/or microconstituents in the microstructure, such as the case in ferritic/pearlitic (F/P) steels, may lead to local separation of cathodic and anodic sites due to the exposure of iron carbide matrix on the steel surface after the dissolution of iron in the ferrite phase.^{6,7}

Farelas, *et al.*,⁸ demonstrated that the presence of a residual iron carbide matrix enhanced the formation of a protective iron carbonate layer. The author reported that the formation of a protective iron carbonate layer was more rapid in the presence of a F/P microstructure of a UNS G10180 steel than in a tempered martensitic microstructure of an API 5L X65 steel when these substrates were exposed to a 3 wt.% NaCl solution saturated with CO₂ at pH of 6.00, temperature of 80°C and fluid velocity of 0.5m/s. The author further stated that in the initial active CO₂ corrosion stage, a cementite matrix, leftover from the dissolution of α -ferrite, formed a structure favorable for the formation of a protective corrosion product layer. Di Bonaventura⁹ showed that the formation of an iron carbonate layer was impeded if this initial iron carbide layer was damaged due to exposure to a high shear stress (above 100Pa). With these findings, the author concluded that iron carbide residues on an actively corroding steel surface can significantly affect the formation of protective corrosion product layers. Putting these findings in the context of a sour environment, and with the general understanding that the formation of FeS occurs rapidly¹⁰⁻¹², it is reasonable to think the film-free stage in H₂S corrosion, if at all present, is short. Therefore, the corrosion process in sour environments may not allow for the formation of significant amount of cementite residues as is the case in CO₂ environments, and may have a reduced significance on the formation of protective iron sulfide layers.

Earlier studies reported a preferential precipitation of iron sulfides on the pearlite region of a steel with a ferrite/pearlite microstructure.^{6,13} It was claimed that since cementite has a lower hydrogen overvoltage than ferrite^{6,14}, the iron dissolution (anodic reaction) occurs in the ferrite while the hydrogen reduction (cathodic reaction) occurs in the cementite phase causing a local increase in pH. However, these claims of preferential precipitation of iron sulfides on pearlite were later refuted by Bai, *et al.*,¹⁵ who reported that FeS layers developed equally on both the pearlite and the ferrite regions when an steel was exposed to H₂O and H₂S at 50°C. These contrary claims on the impact of iron carbide matrix on FeS layer morphology clearly show that there is no consensus on this subject. While it is important to note that the microstructure of steel impacts the morphology of corrosion products, it is even more relevant to investigate how this affects the protectiveness of these layers as has been reported for CO₂ conditions.⁸ Kim, *et al.*,³ compared the morphology of iron sulfide layers formed on pressure vessel steels with F/P and bainitic microstructures. The authors presented cross-section analyses of the corrosion product layers which showed a greater degree of precipitation occurring over pearlite regions. It was concluded that the long-range cementite network found in the F/P microstructure enhanced the attachment of the FeS layer and also provided better protection. The cross-section analyses presented in this study were, however, somewhat vague as the phase occupying the area directly above the pearlite region was not definitively identified as FeS.

The current research investigates the possible effect of iron carbide on the morphology of FeS layers developed on an F/P UNS G10180 in comparison to a 99.9% pure Fe substrate (Surepure Chemetals[‡]). The surfaces and cross-sections of the substrates were analyzed to ascertain any differences in the morphologies of the FeS layers developed after exposure to the test environment. The influence of these layer morphologies on their protectiveness was established by monitoring the corrosion rate trends of UNS G10180 and 99.9% pure Fe in the test solutions. Furthermore, the corrosion product layers developed on the substrate material were analyzed in order to determine the phase composition and identity.

EXPERIMENTAL METHODOLOGY

Equipment

Experiments were conducted in a 4-liter glass cell (Figure 1) which accommodates seven 0.50" x 0.50" x 0.08" square specimens, mounted in holders, with an impeller at the center to induce flow. This system is ideal for this study due to its capability of providing a good control of the solution chemistry, mass transport of species, and generating flow with low shear stresses. One specimen was used for electrochemical measurements and the other six for weight loss and cross-section analyses. A three-electrode system was used for the electrochemical measurements, consisting of a platinized niobium wire counter electrode, an Ag/AgCl reference electrode and the test specimen as the working electrode.

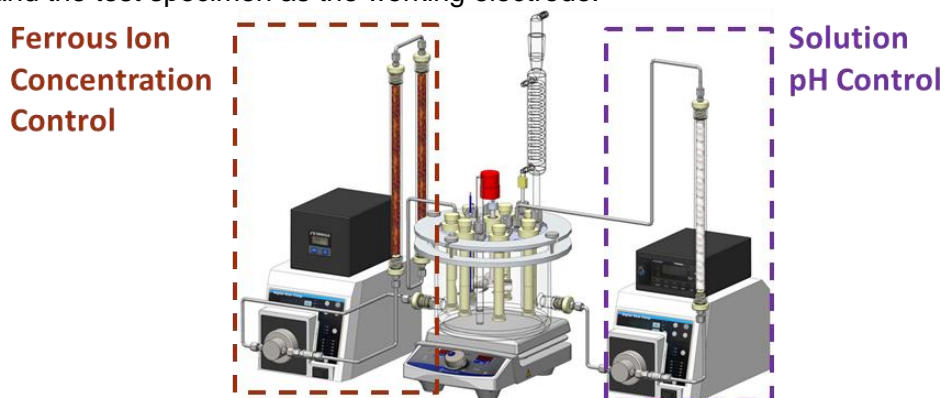


Figure 1: Glass cell with specimen holders, impeller assembly and water chemistry control system

Material Preparation and Microstructure Analysis

The materials used for the current research are commercially sourced 99.9% pure Fe and a UNS G10180 carbon steel material. The chemical composition of the UNS G10180 steel is shown in Table 1.

[‡] Trade name

Table 1
Chemical composition of the UNS G10180 mild steel specimens

UNS G10180 mild steel (wt.%)										
Al	As	C	Co	Cr	Cu	Mn	Mo	Nb	Ni	P
0.008	0.006	0.180	0.003	0.120	0.180	0.750	0.020	0.002	0.065	0.011
S	Sb	Si	Sn	Ta	Ti	V	W	Zn	Zr	Fe
0.021	0.009	0.160	0.009	0.028	0.002	0.003	0.014	0.004	0.003	Balance

Specimens were polished with silicon carbide abrasive paper in the order 150, 400 and 600 grit. While polishing, specimens were rinsed with isopropanol and water to avoid heating up and to remove metal particles and other debris. Specimens were subsequently cleaned by immersion in isopropanol and placed in an ultrasonicator for 5 minutes.

The microstructural analysis of the specimens was conducted by polishing the specimens further with a diamond suspension up to a finish of 0.25 microns. After polishing, specimens were rinsed in deionized water and degreased in isopropanol. Specimens were viewed under an optical microscope to ensure that no debris was present on the surface before being etched in a 5% Nital solution (5% HNO₃ in CH₃OH). The microstructures revealed from etching were examined by scanning electron microscopy (SEM). The same etching procedure was used for cross sectional analysis for all specimens after exposure to the test environment.

Microstructure of Test Specimens

The microstructures of the 99.9% pure Fe and the UNS G10180 carbon steel after etching in a 5% Nital solution are presented in Figure 2 (a.) and (b.), respectively. The etched surface of the 99.9% pure iron specimen shows a single-phase microstructure (ferrite) with large grain size, while the etched UNS G10180 surface revealed a ferritic-pearlitic microstructure. The pearlite constituent has a lamellar structure comprised of alternating cementite and ferrite regions.

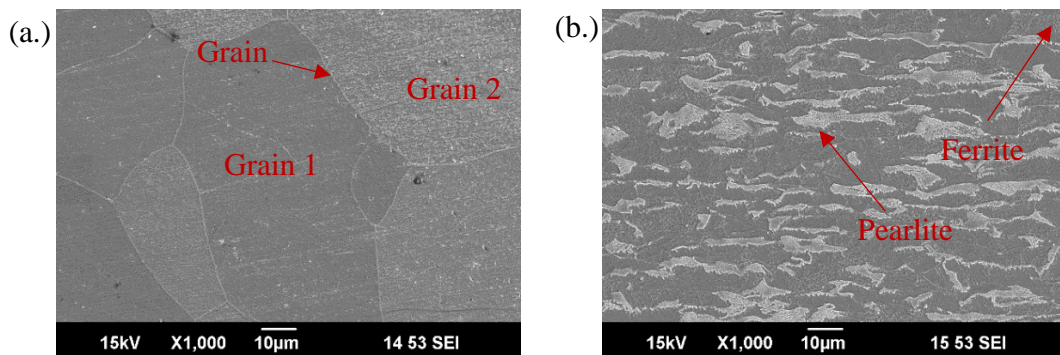


Figure 2: Microstructure of (a.) 99.9% pure Fe substrate (b.) UNS G10180 substrate, revealed after etching in 5% Nital solution, showing phases and grain boundaries.

Test Methodology and Procedure

Specimens were exposed to a 1 wt.% NaCl solution saturated with 10% by volume of H₂S with N₂ as a gas mixture. The system was at atmospheric pressure. The test solution was deoxygenated by sparging with pure N₂ for 2 hours before introducing the desired 10% by volume of H₂S in N₂ gas mixture. The pH of the solution was adjusted to the desired value by adding

drops of deoxygenated 1 molar NaOH solution. During experiments, the pH of the bulk solution was maintained by the solution chemistry control system (Reference). Linear polarization resistance (LPR) measurements were conducted from -5mV to +5mV with a scan rate of 0.125 mV/s during the experiment to observe the trend of the corrosion rate with time (B value = 26mV/dec). Two weight loss specimens were extracted on the first, third and final days of the experiment. At the time of extraction, specimen holders were withdrawn from the solution and the specimens themselves extracted from the holder. Immediately after extraction, the specimens were rinsed in a deoxygenated deionized water to rinse off any salt, further rinsed in isopropanol to remove the water, and dried afterwards in a desiccator under vacuum. Specimens were always stored in a vacuum desiccator prior to analysis. Surface SEM and cross-sectional analysis was conducted on one specimen while weight loss analysis was conducted on the other. The corrosion rates by mass loss were obtained by measuring the mass loss due to corrosion after exposing the specimen to the test solution for a particular time. The mass loss due to corrosion was the difference between the mass of the specimen before exposure and the mass after removal of the corrosion product layer, with Clarke solution¹⁶, following extraction from the test solution. After removal of the corrosion product layer, specimen surfaces were examined for the presence of localized corrosion using profilometry. XRD analysis was conducted on the specimen extracted on the last day.

Test Matrix

Table 2 shows the test matrix for this study. The resistance of the solution was measured using electrochemical impedance spectroscopic method and the value obtained was subtracted from the R_p value obtained from the LPR measurements. The resulting R_p value was used to calculate the corrosion rates.

Table 2
Test Matrix for studying the impact of iron carbide on iron sulfide layer development after 4 days exposure.

Operating Parameter	Specification
Material	99.9% pure iron, UNS G10180
H ₂ S Partial Pressure	0.1 bar
Total Pressure	1.01 bar
Electrolyte	1 wt.% NaCl
Solution pH	5.0, 6.0
Temperature	30°C
Expected FeS Phase	Mackinawite
Impeller Rotational Speed	250rpm
Test Duration	4 days
Measurement Methods	LPR, WL
Surface Analysis	SEM, EDS, XRD, Profilometry

RESULTS AND DISCUSSION

Iron Sulfide Layer Development in Environment Promoting Fe_3C Formation (pH 5.00)

The role of cementite on the development of iron sulfide layer was investigated by exposing UNS G10180 and 99.9% pure Fe to an environment which promoted the formation of Fe_3C . The protectiveness of the layers formed on these two substrates were also investigated.

The solution chemistry in this system was controlled with the pH maintained at 5.00 ± 0.07 , while the Fe^{2+} mass concentration remained below 3.1 ppm throughout the duration of the experiment. At the measured bulk pH and Fe^{2+} concentration, the calculated saturation¹⁷ of FeS in the bulk solution irrespective of the substrate was between the value of 0 and 4 at 30°C .

The corrosion rates measured by weight loss and LPR methods are shown in Figure 3a and Figure 3b, respectively. The tests in this condition were conducted twice and the average of corrosion rates were plotted in the charts shown in Figure 3. The error bars represent the highest and the lowest values from both tests. A comparison was made between the experimentally obtained corrosion rates and a corrosion prediction model developed by Zheng et al.¹⁸ The discussion on how this model is developed can be found in literature.¹⁸

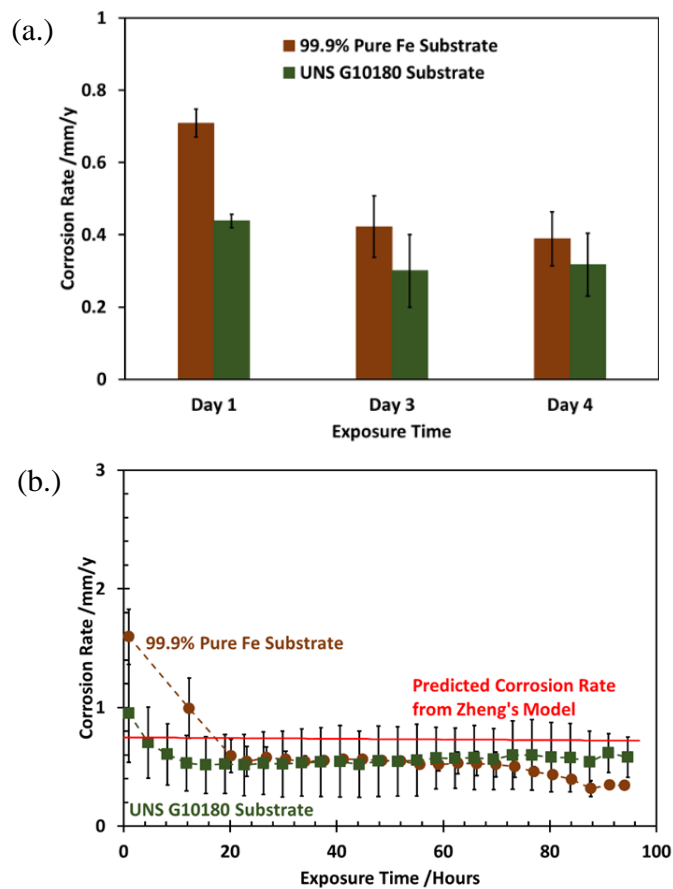


Figure 3: Corrosion rates of 99.9% pure Fe and UNS G10180 in 1 wt.% NaCl solution, at pH 5.00, for 0.1 bar of H_2S , 30°C and impeller rotational speed of 250rpm calculated from (a.) Weight loss measurements and (b.) LPR measurements

In the first day, the corrosion rate of the 99.9% pure Fe substrate was higher than that of the UNS G10180 specimen. In both cases, the corrosion rate decreased sharply due to the formation of corrosion product (FeS) on the substrate surface. The corrosion rate trends from LPR also suggest the corrosion product layer formed on UNS G1018 achieved its maximum protectiveness within the first 14 hours. In comparison, maximum protectiveness of the corrosion product layer formed on 99.9% Fe substrate was achieved in 90 hours. This does not necessarily mean that the layer formed on UNS G10280 was more protective than those formed on the 99.9% pure Fe. Instead, it is likely that the kinetics of iron dissolution or/and cathodic reactions on the 99.9% pure Fe are different from that of UNS G10180. However, with extended exposure time, the development of corrosion product layers progressed, and the corrosion rates of the substrates became similar, especially between 20-60 hours. This observation suggests that, under these conditions, the corrosion product layer is the most important parameter controlling corrosion, and that the presence of the iron carbide network may only increase kinetics of precipitation. No significant change in the open circuit potential was measured during sample exposure. This, along with the corrosion rate trend results, confirms that corrosion processes in sour (H_2S) environments are devoid of a film-free iron dissolution stage as observed in sweet (CO_2) environments.⁸ With the immediate drop in the corrosion rate after the exposure of the specimens to the corrosion environment, FeS layers can be said to rapidly form, cover any iron carbide network that may have developed and also offer some protection to the substrate metal.

Cross-section Analysis of the Corrosion Product Layer

The cross section of the specimens extracted at different exposure times were examined to determine if there were any morphological differences in the corrosion product layers. All cross-section specimens were etched in order to reveal the microstructure of the underlying substrate metal. A thin, continuous corrosion product layer developed after 24 hours exposure time, (Figure 4) irrespective of the substrate metal. However, UNS G10180 specimens extracted after 72 hours and 96 hours (Figure 5 and Figure 6) showed a preferential development of the FeS layer above the pearlite region while the FeS layer developed uniformly on the 99.9% pure Fe substrate. This selective precipitation of iron sulfides in the pearlitic region may also cause local differences in mass transfer rates of corrosive species to the surface. Lower pH conditions which may favor higher exposure of pearlites in the steel microstructure would result in low FeS saturation and precipitation. Therefore, further investigation was conducted in at higher pH.

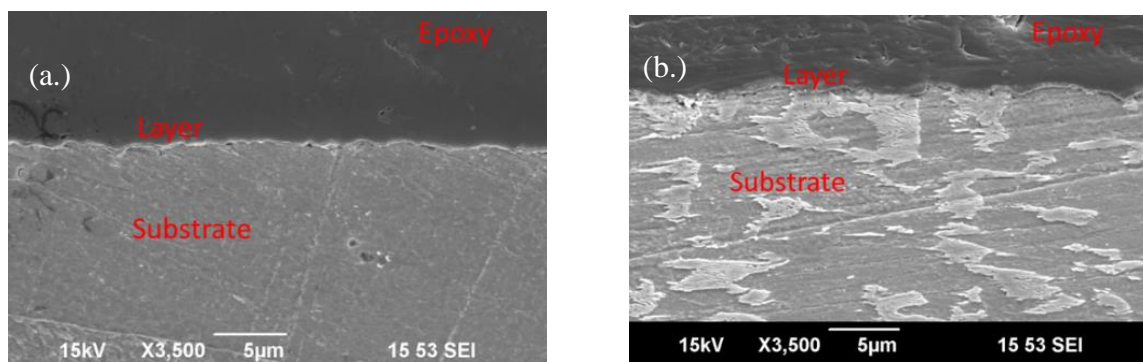


Figure 4: Cross-section of FeS layer formed after 1 day exposure in 1 wt.% NaCl solution at 30°C, at pH 5.00, for 0.1bar of H_2S and 250rpm impeller rotational speed (a.) 99.9% pure Fe substrate (b) UNS G10180 substrate.

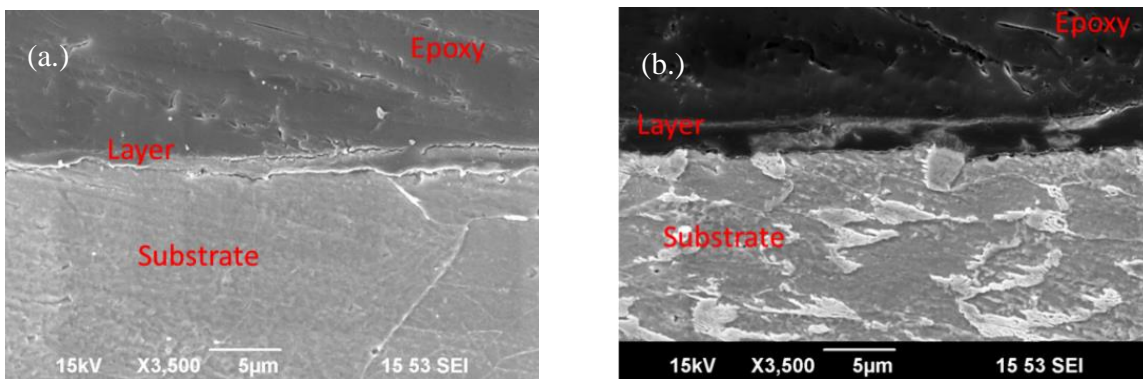


Figure 5: Cross-section of FeS layer formed after 3 days exposure in 1 wt.% NaCl solution at 30°C, at pH 5.00, for 0.1bar of H₂S and 250rpm impeller rotational speed (a.) 99.9% pure Fe substrate (b) UNS G10180 substrate.

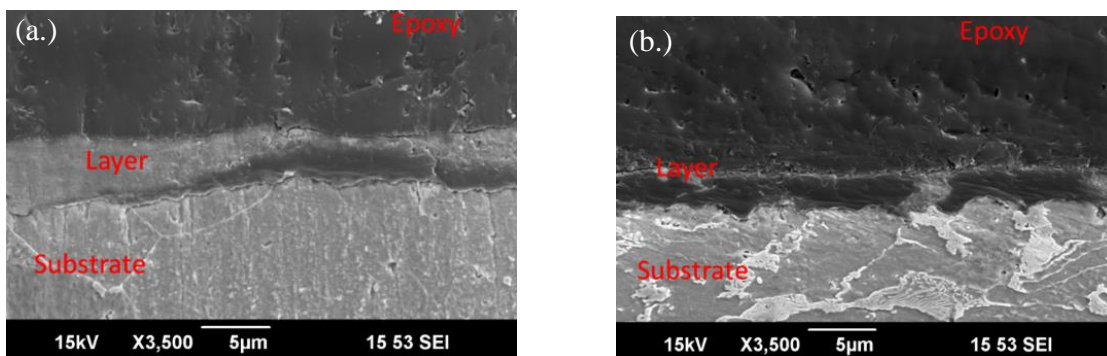


Figure 6: Cross-section of FeS layer formed after 4 days exposure in 1 wt.% NaCl solution at 30°C, at pH 5.00, for 0.1bar of H₂S and 250rpm impeller rotational speed (a.) 99.9% pure Fe substrate (b) UNS G10180 substrate.

Different authors have reported that the presence of a pearlite structure favors the formation of protective corrosion product layers.^{3,6} In CO₂ environments, it was postulated that the enhanced FeCO₃ formation is a result of an increase in its local saturation degree within the iron carbide matrix, which provides both structural support and a favorable solution for the growth of the layer.^{8,9,19} Irrespective of the environment, (H₂S or CO₂), a local galvanic couple can also formed between the iron carbide present in the pearlite region and the ferrite, where the iron carbide acts as a cathode and the ferrite as the anode¹⁴. In H₂S environment, the major cathodic reactions on the cementite phase are the hydrogen ion reduction and hydrogen sulfide reduction reactions. Ferrous ion dissolution, which occurs at the anode, is accelerated in the pearlite region due to the existence of the local galvanic couple in this region. In order to maintain electroneutrality, an increase in the ferrous ion concentration causes a decrease in the hydrogen ion concentration; and consequently, an increase in the local pH. With reference to the saturation expression,^{18,20} an increase in the pH and ferrous iron concentration in the pearlite region favors the formation of FeS layers in this area.

Surface Analysis of Corrosion Product Layers

XRD analyses conducted after 4 days detected strong mackinawite peaks with the 99.9% pure Fe substrate (Figure 7). This may be due to the dense nature of the corrosion product layer that developed on the pure iron substrate as shown in the cross-section images presented earlier.

Surprisingly, no mackinawite peak was detected with the UNS G10180, but this may be due to the very low thickness of the layer formed. It should also be noted that iron carbide peaks were not detected in the XRD spectrum which might suggest that the complete coverage of this matrix by FeS was achieved. This is in contrast to observations in CO₂ conditions⁹, where iron carbides were detected by XRD even in the presence of iron carbonates.

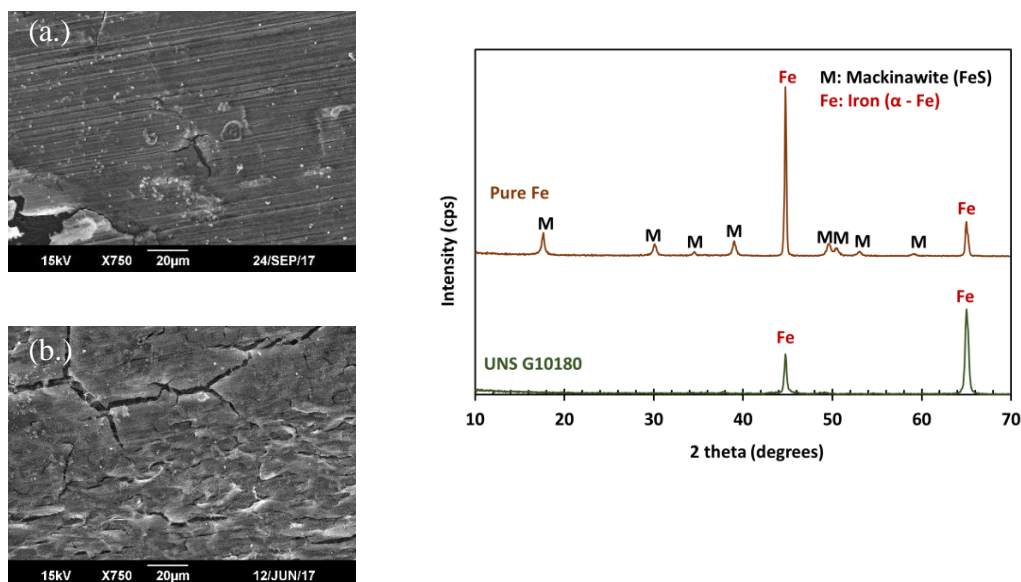


Figure 7: SEMs and XRD analyses of corrosion product layers formed on (a.) 99.9% pure Fe and (b.) UNS G10180 after a 4 day exposure in 1 wt. % NaCl solution, at pH 5.00, and for 0.1bar of H₂S at a system temperature of 30°C and impeller rotational speed of 250rpm

Iron Sulfide Layer Development under High FeS Saturation (pH 6.00)

Further experiments were conducted at pH 6.00, where a higher precipitation rate was expected due to the increase in bulk FeS saturation. The bulk solution pH and ferrous ion concentration during the period of the experiment were also measured. The mass concentration of ferrous ion was lower than 1ppm (lower than that measured in pH 5.00 conditions). This is expected since, at pH 6.00, the decreased hydrogen ion concentration shifts the equilibrium of the FeS saturation reaction towards the product (FeS),^{18,20} leading to a higher precipitation rate of FeS.

The corrosion rates measured by weight loss and LPR methods under these conditions are shown in Figure 8a and Figure 8b, respectively. Corrosion rates trends were also compared with the prediction from the Zheng model¹⁸. A B-value of 26mV/decade of current was used in both the LPR corrosion calculation and Zheng's model¹⁸. The prediction model showed good agreement with the LPR and weight loss corrosion rates for the carbon steel. However, with pure Fe, the corrosion rates from LPR were consistently higher than both the predicted value and the weight loss. This difference can be attribute to the B-value used which is more suited for carbon steel specimens. Tests were conducted twice, and the average of corrosion rates were plotted in the charts shown in Figure 4. The error bars represent the highest and the lowest values from both tests. The large errors bars in the weight loss corrosion rates may be indicative of the variation in the protective properties of the corrosion product layer formed in this condition.

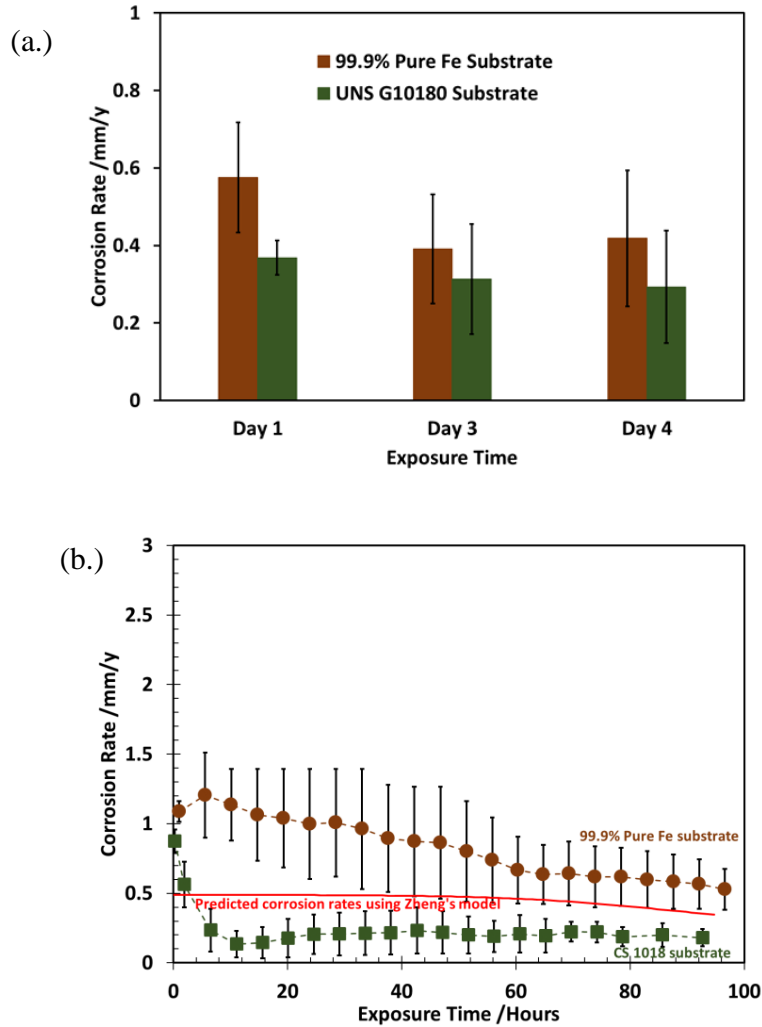


Figure 8: Corrosion rates of 99.9% pure Fe and UNS G10180 in 1 wt.% NaCl solution, at pH 6.00, for 0.1 bar of H₂S, 30°C and impeller rotational speed of 250rpm calculated from (a.) weight loss measurements and (b.) LPR measurements

The corrosion rate of UNS G10180 reached a stable value of approximately 0.2mm/y within the first 10 hours of specimen exposure, 4 hours earlier than it did at pH 5.0. However, the corrosion rates of the 99.9% pure Fe substrate continued to gradually decrease throughout the period of exposure. This shows that UNS G10180 developed a protective FeS layer faster than the pure Fe substrate, which highlights the importance of the iron carbides in the protectiveness of FeS layers in the low shear stress condition.

The increase in the open circuit potential typically associated with pseudo-passivation^{21,22} of a mild steel substrate was observed with only UNS G10180 substrate (Figure 9). This may be an indication of a better attachment of the FeS layers facilitated by the iron carbides.

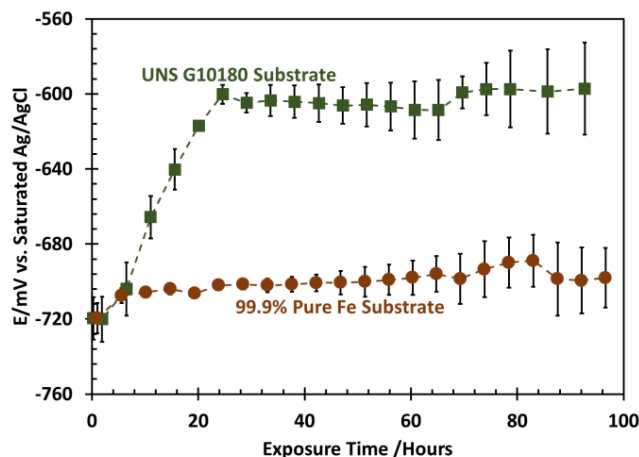


Figure 9: Open circuit potential (vs. Ag/AgCl) of 99.9% pure Fe, and UNS G10180, in 1 wt.% NaCl solution, at pH 6.00, for 0.1 bar of H₂S, 30°C and impeller rotational speed of 250rpm

Cross-section Analysis of the Corrosion Product Layer

Figure 10 – 14 show the cross-sections of the corrosion product layers developed on 99.9% pure Fe and UNS G10180 after 1, 3 and 4 days of exposure in the test solution.

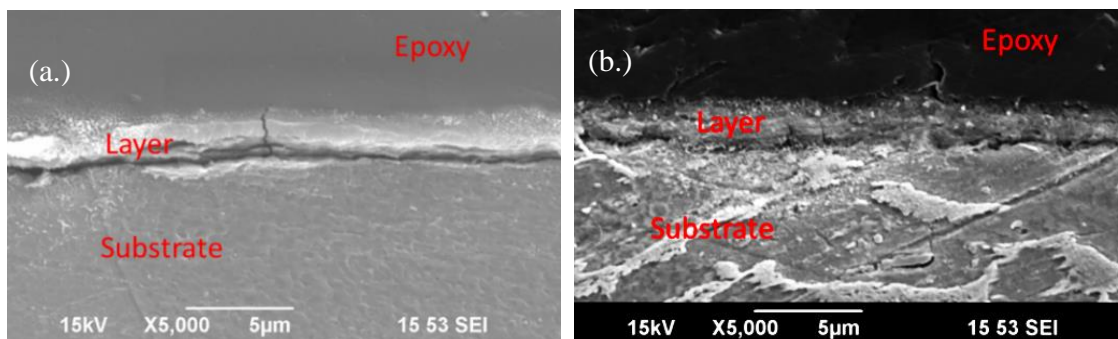


Figure 10: Cross-section of FeS layer formed after 1-day exposure in 1 wt.% NaCl solution at 30°C, at pH 6.00, for 0.1bar of H₂S and 250rpm impeller rotational speed (a.) 99.9% pure Fe substrate (b) UNS G10180 substrate.

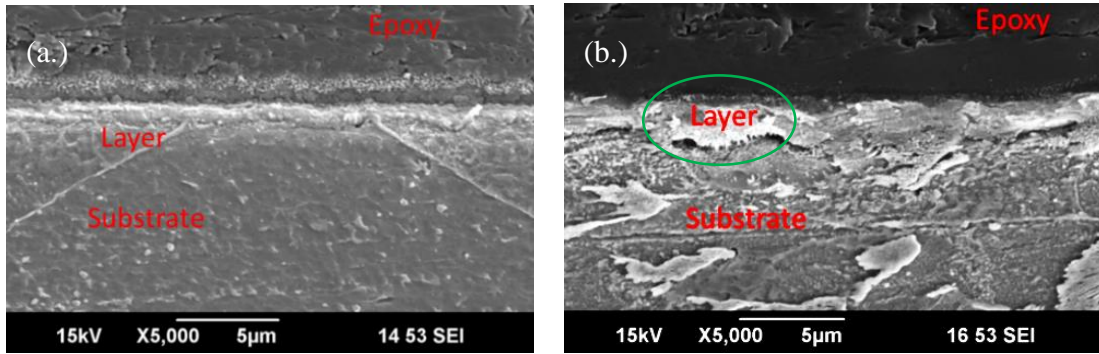


Figure 11: Cross-section of FeS layer formed after 3 days exposure in 1 wt.% NaCl solution at 30°C, at pH 6.00, for 0.1bar of H₂S and 250rpm impeller rotational speed (a.) 99.9% pure Fe substrate (b) UNS G10180 substrate.

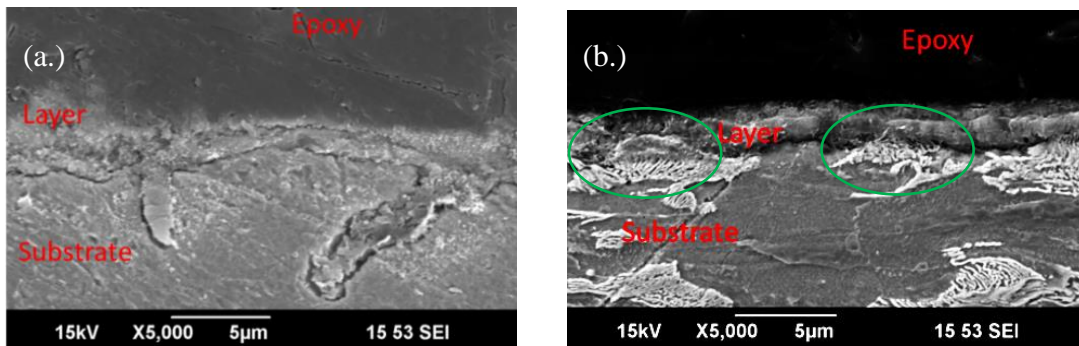


Figure 12: Cross-section of FeS layer formed after 4 days exposure in 1 wt. % NaCl solution at 30°C, at pH 6.00, for 0.1bar of H₂S and 250rpm impeller rotational speed (a.) 99.9% pure Fe substrate (b) UNS G1018 substrate.

These cross-sections showed similarities in the overall morphologies of the corrosion product layers. The iron sulfide layer present on the 99.9% pure Fe surface seemed to be thin and continuous. A closer observation of the FeS layer formed over the pearlite regions of UNS G10180, especially on samples extracted after 3 and 4 days (highlighted with green circles), shows the FeS layers filling-up the cementite skeletal framework as well as the gaps between them. However, the corrosion rate trends and OCP (Figure 8 and Figure 9) infer that the presence of iron carbide enabled the formation of a continuous iron sulfide layer and promoted the attachment of this layer. Bai, *et al.*,¹⁵ demonstrated that the precipitation rate of the FeS layers was higher over the pearlite area when a ferritic/pearlitic steel was exposed to an H₂S saturated NACE TM0284-96A solution with an initial pH of 2.8. It was also reported that the iron sulfide layers formed on the steel with F/P microstructure provided more protectiveness when compared to a layer developed on a steel with a bainitic microstructure exposed to the same environment. These reported behaviors of F/P steels support the findings from the current study at pH 5.00 and especially at pH 6.00 conditions.

Surface Analysis of Corrosion Product Layers

Figure 13 shows the results from the EDS spot analysis of the FeS layer formed within the pearlite and those that formed on other areas of the specimen. The spots of the EDS were scaled to the actual size of the spot area from where data was collected.

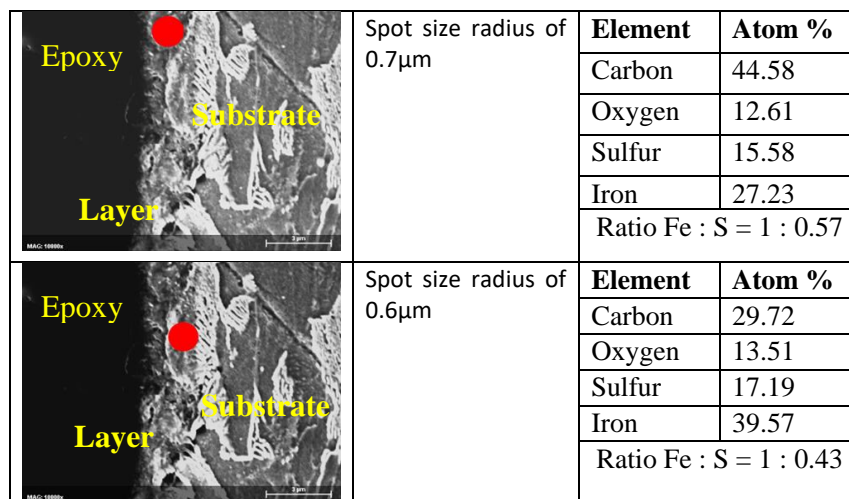


Figure 13: EDS spot analysis of the layer at different locations on the UNS G10180 substrate after 4 days exposure period in 1 wt.% NaCl solution at 30°C, pH 6.00, 0.1bar of H₂S and 250rpm impeller rotational speed (a.) outside the pearlite region (b.) in the pearlite region

The percentage carbon content of the layer formed in the pearlite region was lower than that formed outside the pearlite region. Since the main source of carbon is the epoxy, it can be inferred that the layers with the lower % carbon content are more compact than those with higher carbon content. The layer formed above the pearlite region may be denser and more compact than the FeS layer formed in other areas on the specimen. The XRD analysis (Figure 14) shows similar mackinawite peaks for the layers formed on 99.9% pure Fe.

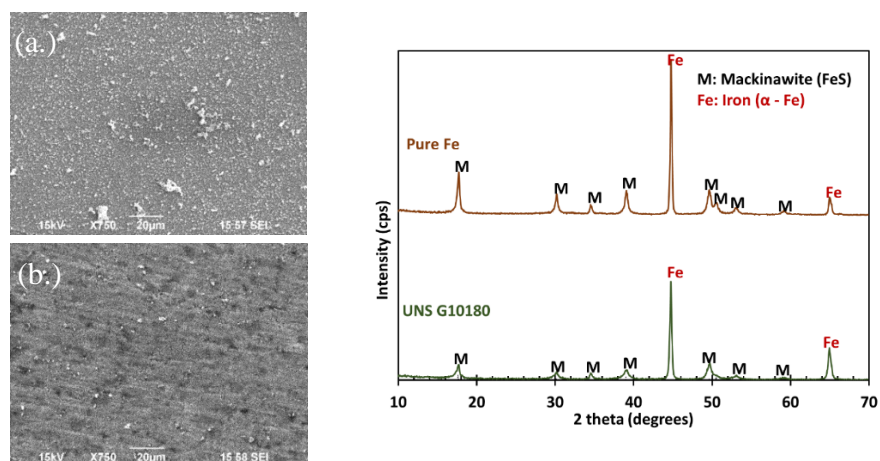


Figure 14: XRD analyses of corrosion product layers formed on (a.) 99.9% pure Fe and (b.) UNS G10180 after 4 days exposure in 1 wt.% NaCl solution, pH 6.00, and 0.1 bar of H₂S at system temperature of 30°C and impeller rotational speed of 250rpm

Figure 12a also revealed an area with an accelerated corrosion which raised the suspicion of localized attack. The surfaces of the exposed metals were examined using a profilometer to detect any possible occurrence of localized corrosion (Figure 15 and Figure 16).

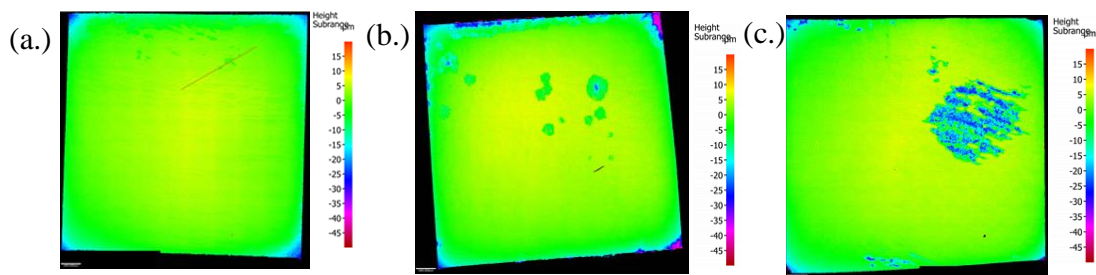


Figure 15: Topography of 99.9% pure Fe surface after removing the corrosion product layer with Clarke solution after exposure times of (a.) 1 day (b.) 3 days and (c.) 4 days.

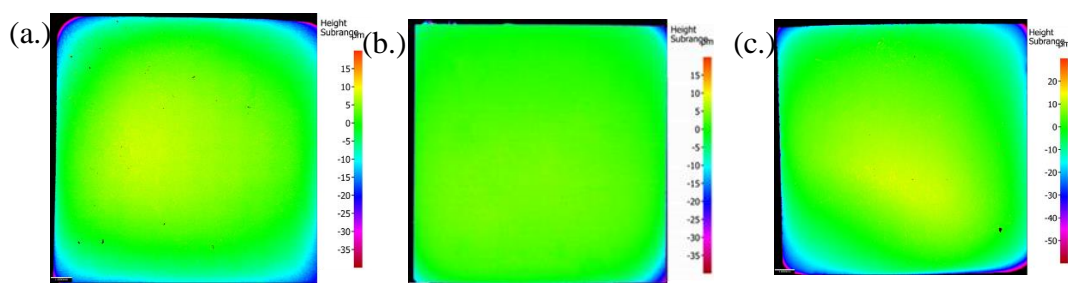


Figure 16: Topography of UNS G10180 surface after removing the corrosion product layer with Clarke solution after exposure times of (a.) 1 day (b.) 3 days and (c.) 4 days.

The mapped topography of the specimen surfaces presented in Figure 15 and Figure 16 showed the possible occurrence of localized attacks on the pure Fe substrate and uniform corrosion occurred on the UNS G10180 substrate. However, these localized attacks could not be reproduced. The repeat experiment showed an unevenly corroded surface after 4 days of exposure of the pure Fe substrate. Therefore, the occurrence of localized corrosion on the 99.9% pure Fe substrate in the current test environment cannot be inferred. However, the difference in the surface profile of the substrates after the removal of the corrosion product layers suggests that, under the current experimental condition, the layers had a better attachment on the UNS G10180 substrate in comparison to the 99.9% pure Fe substrate.

CONCLUSION

The role of iron carbide on the corrosion behavior of a ferritic/pearlitic carbon steel was investigated by exposing UNSG 10180 and 99.9% pure Fe material to brine solutions sparged with 10% by volume of H₂S in a mixture with nitrogen, at temperature of 30°C and pH of 5.00 and 6.00 for a period of 4 days. Results from this study suggests that the early stage of the corrosion process involves the fast formation of an initial thin and continuous mackinawite layer. After this early stage, the corrosive species diffuses through this initial thin mackinawite layer to get the metal surface. At this stage the iron carbide in the steel microstructure becomes critical to its corrosion behavior due to its influence on the precipitation of the FeS on the metal surface. This was most evident in samples formed after 3 and 4 days in pH 5.0 solutions (Figure 5 and Figure 6). While the presence of an iron carbide matrix enhances the adherence of the FeS layer on the UNS G10180 steel surface, the FeS layers formed on pure Fe substrate were more loosely attached and may have promoted undermining corrosion. The later stages of the FeS development on UNS G10180 is associated with high precipitation rates of FeS and complete

coverage of the surface by FeS. A higher precipitation preferentially occurs at the pearlite microconstituents as indicated by the green circles in Figure 11 and Figure 12.

Based on the results and observations from the current study, the following were concluded:

- The corrosion process in H₂S conditions lacks the active corrosion stage present in CO₂ conditions.
- The presence or absence of Fe₃C does not affect the final steady state corrosion rate.
- The presence of Fe₃C promotes precipitation of FeS in the pearlite region.
- The presence of Fe₃C affects the layer morphology and characteristics, promoting the attachment of FeS to the metal surface and leading to a comparatively sharper decrease in the corrosion rates.
- The pure Fe substrate showed possible susceptibility to localized corrosion at solution pH 6.00. However, the evidence was not fully conclusive as the occurrence of localized corrosion could not be repeated.

These findings suggest that the use of pipeline steel with ferritic/pearlitic microstructure in sour environment may enhance the protectiveness of the corrosion product layers that may form in this environment and favor a longer service life of structures.

REFERENCE

- [1] E. J. Pavlina and C. J. Van Tyne, "Correlation of Yield strength and Tensile strength with hardness for steels," *J. Mater. Eng. Perform.*, vol. 17, no. 6, pp. 888–893, Dec. 2008.
- [2] T. G. Digges, S. J. Rosenberg, and G. W. Geil, "Heat Treatment and Properties of Iron and Steel," *US Dept of Commerce*.1966.
- [3] S. J. Kim, J. H. Park, and K. Y. Kim, "Effect of microstructure on sulfide scale formation and corrosion behavior of pressure vessel steel in sour environment," *Mater. Charact.*, vol. 111, pp. 14–20, Jan. 2016.
- [4] A. Dugstad, H. Hemmer, and M. Seiersten, "Effect of Steel Microstructure on Corrosion Rate and Protective Iron Carbonate Film Formation," *Corrosion Journal*, vol. 57, no. 4, pp. 369–378, Apr. 2001.
- [5] D. Clover, B. Kinsella, B. Pejicic, and R. De Marco, "The influence of microstructure on the corrosion rate of various carbon steels," *J. Appl. Electrochem.*, vol. 35, no. 2, pp. 139–149, Feb. 2005.
- [6] H.-H. Huang, W.-T. Tsai, and J.-T. Lee, "Electrochemical behavior of the simulated heat-affected zone of A516 carbon steel in H₂S solution," *Electrochim. Acta*, vol. 41, no. 7–8, pp. 1191–1199, May 1996.
- [7] S. Nestic, Y. Zheng, B. Brown, and J. Ning, "Advancement in Predictive Modeling of Mild Steel Corrosion in CO₂ and H₂S Containing Environments," in *Corrosion Conference Proceedings*, no. 6146, Dallas: NACE, 2015.
- [8] F. Farelas, B. Brown, and S. Nestic, "Iron Carbide and its Influence on the Formation of Protective Iron Carbonate in CO₂ Corrosion of Mild Steel," in *Corrosion Conference Proceedings*, no. 2291, Orlando: NACE, 2013.
- [9] M. C. Di Bonaventura, "Effect of Flow on the Formation of Iron Carbonate and Influence of Exposed Iron Carbide Layer," Ohio University, 2017.
- [10] Y. Zheng, J. Ning, B. Brown, D. Young, and S. Nestic, "Mechanistic study of the effect of iron sulfide layers on hydrogen sulfide corrosion of carbon steel," in *Corrosion Conference Proceedings*, no. 5933, Dallas: NACE, 2015, pp. 1–20.
- [11] W. Sun, S. Nestic, S. Papavinasam, and others, "Kinetics of iron sulfide and mixed iron

- sulfide/carbonate scale precipitation in CO₂/H₂S corrosion,” in *Corrosion Conference Proceedings*, no. 06644, San Diego: NACE, 2006.
- [12] W. Sun, “Kinetics of Iron Carbonate and Iron Sulfide Scale Formation In CO₂/H₂S Corrosion,” Ohio University, 2006.
- [13] A. M. Zimer *et al.*, “Investigation of AISI 1040 steel corrosion in H₂S solution containing chloride ions by digital image processing coupled with electrochemical techniques,” *Corros. Sci.*, vol. 53, no. 10, pp. 3193–3201, Oct. 2011.
- [14] R. W. Revie and H. H. Uhlig, *Corrosion and corrosion control: An introduction to corrosion science and engineering*, 4th ed. Canada: A John Wiley & Sons, Inc., Publication, 2008.
- [15] P. Bai, H. Zhao, S. Zheng, and C. Chen, “Initiation and developmental stages of steel corrosion in wet H₂S environments,” *Corros. Sci.*, vol. 93, pp. 109–119, 2015.
- [16] “Standard Practice for Preparing, Cleaning, and Evaluating Corrosion Test Specimens,” *ASTM Stand. G 1 - 90*, 1999.
- [17] J. Ning, Y. Zheng, D. Young, B. Brown, and S. Nešić, “A Thermodynamic Study of Hydrogen Sulfide Corrosion of Mild Steel,” in *Corrosion Conference Proceedings*, no. 2462, Orlando: NACE, 2013.
- [18] Y. Zheng, “Electrochemical Mechanism and Model of H₂S Corrosion of Carbon Steel,” Ohio University, 2014.
- [19] M. Di Bonaventura, B. Brown, M. Singer, and S. Nesic, “Effect of Flow and Steel Microstructure on the Formation of Iron Carbonate,” in *Corrosion Conference Proceedings*, no. 11179, Phoenix: NACE, 2018.
- [20] Z. Ma, Y. Yang, B. Brown, S. Nesic, and M. Singer, “Investigation of FeCO₃ and FeS Precipitation Kinetics by EQCM,” in *Corrosion Conference Proceedings*, no. 11192, Phoenix: NACE, 2018.
- [21] J. Han, S. Nešić, Y. Yang, and B. N. Brown, “Spontaneous passivation observations during scale formation on mild steel in CO₂ brines,” *Electrochim. Acta*, vol. 56, no. 15, pp. 5396–5404, Jun. 2011.
- [22] W. Li, B. Brown, D. Young, and S. Nešić, “Investigation of Pseudo-Passivation of Mild Steel in CO₂ Corrosion,” *Corrosion Journal*, vol. 70, no. 3, pp. 294–302, Mar. 2014.